

1 COUPLING MODIS AND RADAR ALTIMETRY DATA FOR DISCHARGE  
2 ESTIMATION IN POORLY GAUGED RIVER BASINS

3 A. Tarpanelli<sup>1</sup>, L. Brocca<sup>1</sup>, S. Barbeta<sup>1</sup>, M. Faruolo<sup>2</sup>, T. Lacava<sup>2</sup>, T. Moramarco<sup>1</sup>

4 <sup>1</sup> *Research Institute for Geo-Hydrological Protection, National Research Council, Via Madonna Alta 126, 06128 Perugia, Italy*

5 <sup>2</sup> *Institute of Methodologies for Environmental Analysis, National Research Council, C.da Santa Loja, 85050 Tito Scalo (PZ), Italy*

6 ABSTRACT

7 The capability of coupling measurements of river velocity derived from Moderate Resolution  
8 Imaging Spectroradiometer (MODIS) and water levels derived from ENVISAT Advanced Radar  
9 Altimeter (RA-2) for river discharge estimation is thoroughly investigated. The method is applied  
10 even considering the possible unavailability of the river cross-section survey by using the entropy  
11 theory for reconstructing the bathymetry. The discharge estimation accuracy is validated using *in-situ*  
12 measurements along the Po River (Northern Italy) where daily observations are available for the  
13 period 2005-2010.

14 The agreement with the observed discharge is fairly satisfactory with coefficient of correlation  
15 of 0.91 and relative root mean square error of ~ 37% on average. Therefore, the coupling of the two  
16 sensors provides, with a good level of accuracy, the hydraulic quantities to use for discharge  
17 estimation. These results are particularly significant for the forthcoming European Space Agency  
18 Sentinel-3 mission, in which a visible-near infrared multispectral sensor and an altimeter will be  
19 onboard the same satellite platform providing significant improvements in terms of vertical accuracy  
20 and spatial-temporal resolution.

21

22 **Key Words:** MODIS, radar altimetry, remote sensing, discharge, flow velocity, Po River.

---

<sup>1</sup> Corresponding author: Angelica Tarpanelli: Research Institute for Geo-Hydrological Protection, National Research Council, Via Madonna Alta 126, 06128 Perugia, Italy; [a.tarpanelli@irpi.cnr.it](mailto:a.tarpanelli@irpi.cnr.it); phone: +39 0755014426

## 23 1. INTRODUCTION

24 Over the past two decades the availability of remote sensing data has steadily increased and the  
25 number of studies demonstrating the potential of satellite in hydrology has grown rapidly (Alsdorf et  
26 al., 2007; Bjerklie et al., 2003; Smith and Pavelsky, 2008). In particular, the recent advances in radar  
27 altimetry technology by TOPEX/Poseidon (TP), European Remote-Sensing Satellite 2 (ERS-2) and  
28 the Environmental Satellite (ENVISAT) mission offered important information for water levels  
29 monitoring of large rivers, lakes and floodplains (Koblinsky et al., 1993; Birkett, 1998; De Oliveira  
30 Campos et al., 2001; Frappart et al., 2006; Leon et al., 2006; Zakharova et al., 2006; Santos da Silva  
31 et al., 2010; Getirana et al., 2009; Birkinshaw et al., 2010; Michailovsky et al., 2013; Getirana et al.,  
32 2013). For large rivers in continental environment, as the Amazon, the radar altimetry reaches an  
33 accuracy of 30 cm in terms of root mean square error, *RMSE*, as shown by Frappart et al. (2006) and  
34 Santos da Silva et al. (2010) who analyzed data from the Advanced Radar Altimeter (RA-2) onboard  
35 ENVISAT. With the future SWOT (Surface Water Ocean Topography) mission the remote water  
36 level identification will reach an accuracy up to 10 cm also for smaller rivers (width of ~ 100 m)  
37 (Durand et al., 2010; Biancamaria et al., 2010; Fu et al., 2012; Yoon et al., 2013).

38 For very large river basins (>10,000 km<sup>2</sup>) microwave sensors have been already used for  
39 improving discharge monitoring activities (Brakenridge et al., 2007; Temimi et al., 2007, 2011). For  
40 example, Advanced Microwave Scanning Radiometer for the Earth Observing System (AMSR-E)  
41 data have been used by Brakenridge et al. (2007) for the Global Flood Detection System, in order  
42 to globally infer floods also for ungauged and inaccessible rivers  
43 (<http://old.gdacs.org/flooddetection/overview.aspx>). The technique is based on the changes in  
44 brightness temperature between wet measurement pixels (*M*) centered over rivers and dry calibration  
45 pixels (*C*) that are not affected by the river. River flooding is detected by comparing the signal from  
46 the wet pixel and the one from the calibration pixel. Khan et al. (2012) used this technique for the  
47 calibration of a distributed hydrological model with satisfactory results showing that remote sensing

48 data from microwave sensors could be used to supplement stream gauges in large sparsely gauged or  
49 ungauged basins. The same technique, applied to optical Moderate Resolution Imaging  
50 Spectroradiometer (MODIS) data, was also used for river discharge estimation in a preliminary study  
51 by Brakenridge and Anderson (2006). Specifically, the different behavior of water and land in the  
52 Near Infrared (NIR) portion of the electromagnetic spectrum is exploited by computing the ratio of  
53 the MODIS channel 2 reflectance values between two pixels located within and outside the river. The  
54 values of the ratio increase with the presence of water and, hence, with discharge.

55 Two recent studies (Tarpanelli et al., 2013a; 2013b) have investigated the use of sensors like  
56 radar altimetry and MODIS for the discharge evaluation in the Po River (~70,000 km<sup>2</sup>) in northern  
57 Italy. In particular, Tarpanelli et al. (2013a) applied a simple flood routing model for the estimation  
58 of discharge in two river sections along the Po using water level observations by satellite radar  
59 altimetry. The knowledge of discharge at an upstream river section is needed in order to apply the  
60 procedure. Tarpanelli et al. (2013b) showed that MODIS can give satisfactory estimates of velocity  
61 and discharge and that the method can be extended for ungauged river sites. However, the discharge  
62 is evaluated considering the water level measured in the gauged stations, where the cross-sections  
63 survey is available. Therefore, in both approaches in situ observations (upstream discharge or water  
64 level) were used with the purpose of discharge estimation from remote sensing. Additionally, both  
65 the procedures need the cross-section geometry to be applied..

66 On this basis, we present a study in which for the first time two satellite sensors working in two  
67 different spectral regions and with a different technology are coupled for providing discharge  
68 estimation in ungauged section without the knowledge of bathymetry of the cross-sections. Generally  
69 speaking, the discharge is given by the product of the river velocity and the flow area that can be  
70 derived as a function of the water level when the river section geometry is known. Differently from  
71 Tarpanelli et al. (2013a; 2013b), both these hydraulic quantities were derived, in this work, by satellite  
72 measurements. The mean flow velocity was calculated considering the MODIS sensor (Tarpanelli et  
73 al., 2013b), while the water levels, used for the flow area computation, was inferred from the

74 ENVISAT altimeter data. Moreover, if the river section geometry is unknown, the entropy method  
75 proposed by Moramarco et al. (2013) may be used for reconstructing the cross-section flow area from  
76 the flow velocity (estimated by MODIS). This approach may be conveniently applied in poorly  
77 gauged or ungauged river where *in-situ* data are scarce, inaccessible or absent.

78 The Po River (in Northern Italy), where daily *in-situ* water level and discharge observations are  
79 available, is used in this work as a case study. *In-situ* and satellite-derived discharge data are  
80 compared in order to assess the reliability of the proposed procedure.

## 81 2. METHODOLOGY

### 82 2.1 Water level derived by radar altimeter data

83 In order to evaluate the accuracy of altimetry data a preliminary analysis was carried out by  
84 comparing the satellite water level observations with *in-situ* water level measurements. ENVISAT  
85 RA-2 provides a water level time series at the virtual station (VS), i.e. the location where the satellite  
86 track intersects the river reach, with 35-day time interval, while (*in-situ*) discharge and water level  
87 data are available at daily temporal scale. Therefore, for the data comparison, the water levels  
88 measured *in-situ* are selected in temporal correspondence of the acquisition dates of the satellite  
89 sensor overpasses. The comparison between the water level time series, observed at a gauged station  
90 and derived by altimetry, was carried out removing the temporal average values computed  
91 considering both the whole time series (Tourian et al., 2013).

### 92 2.2 Flow velocity estimation by using MODIS data

93 For a detailed description of the approach we refer the reader to Tarpanelli et al. (2013b). In  
94 what follows, only a brief synthesis is reported. Following the studies of Brakenridge and Anderson  
95 (2006) and Brakenridge et al. (2007), we exploit the different behavior of water and land in the Near  
96 Infrared (NIR) portion of the electromagnetic spectrum (MODIS channel 2). Specifically, in the NIR  
97 region, the reflectance values of the water pixel are lower than the ones of the common land pixel and

98 whenever the water surface level increases (i.e. during flood events) affecting a wider portion of the  
99 pixel, a further reduction of the reflectance value of the investigated area has to be expected. These  
100 reflectance measurements are affected by significant noise induced by atmospheric factors. Over a  
101 large area this noise may be minimized by calculating the ratio between the surface reflectance of a  
102 land pixel ( $C$ ) and a water river pixel ( $M$ ). The ratio is sensitive to the increased water level within  
103 the river as well as to the presence of wet areas in the analysed pixel and, hence, of discharge (i.e.  
104 flow velocity). The procedure used in this study can be summarized in the following five steps:

105       **1.** from each MODIS image we selected the box centered in the investigated area, that is the  
106 VS, for which the water levels derived by radar altimetry are available;

107       **2.** the pixels affected by cloud cover and/or snow are identified both by using a fixed threshold  
108 on reflectance values of the first channel,  $R_1$  ( $R_1 > 0.2$ ) and a visual inspection and then excluded from  
109 the analysis;

110       **3.** the position of pixels  $C$  and  $M$  is chosen following the guidelines described in Tarpanelli et  
111 al. (2013b) for ungauged sites and the ratio between the temporal series of the reflectance values of  
112 the second channel  $R_2$  corresponding to the two pixels is calculated;

113       **4.** since the trend of the ratio  $C/M$  appears quite noisy due to the high variability of the surface  
114 reflectance values, the exponential smoothing filter (Albergel et al., 2008; Wagner et al., 1999) is  
115 applied to reduce this effect, obtaining  $C/M^*$ .

116       The regional relationship

$$117 \quad v = 0.56 \cdot C/M^* - 0.03 \quad (1)$$

118 proposed by Tarpanelli et al. (2013b) between the reflectances ratio  $C/M^*$  and the mean flow velocity,  
119  $v$ , derived by using MODIS data at four river reaches along the Po River is here used for obtaining  
120 the velocity at the VS after that the ratio  $C/M^*$  is estimated.

### 121 **2.3 River discharge estimation integrating MODIS and altimetry data**

122 The discharge is assessed by multiplying the mean flow velocity by the flow area calculated as  
123 a function of the water level. If the cross section survey is known, we may use the MODIS ratio,  
124  $C/M^*$ , to derive the mean flow velocity from the regional relationship, and the water level,  $h$ , derived  
125 from the altimetry data for the evaluation of the flow area,  $A$ , from the  $A(h)$  relationship.

### 126 **2.4 River cross-section estimation**

127 If the river cross-section is unknown, the entropy-approach as proposed by Moramarco et al.  
128 (2013) is applied. This method allows determining the flow depth distribution in a natural channel  
129 and it is used here for the cross-sectional estimation of the flow area. For each measurement the  
130 method requires the surface velocity, the maximum flow depth and the channel width. In detail, the  
131 flow depth distribution,  $d$ , along the horizontal distance  $x$  from the vertical  $y$ -axis ( $x=0$ ), where the  
132 maximum surface velocity across the river,  $v_{maxS}$ , occurs, is given by

$$133 \quad d(x) = \frac{D}{W} \ln \left[ \frac{e^W - 1}{v_{maxS}} v_s(x) + 1 \right] \quad (1)$$

134 where  $W$  is a parameter,  $D$  is the maximum flow depth and  $v_s$  is the surface water velocity for each  
135 vertical that is calculated as a function of  $v_{maxS}$  assuming an elliptical or parabolic profile (Moramarco  
136 et al., 2011).

137 In Moramarco et al. (2013), the ratio between the mean and the maximum flow depth,  $H_m/D$  is  
138 assumed given by:

$$139 \quad \frac{H_m}{D} = \left( \frac{e^W}{e^W - 1} - \frac{1}{W} \right) \quad (2)$$

140  $H_m$  can be also obtained integrating the Equation (1) across the whole flow area:

$$141 \quad H_m = \frac{1}{L} \int_0^L \frac{D}{W} \ln \left[ \frac{e^W - 1}{v_{maxS}} v_s(x) + 1 \right] dx \quad (3)$$

142 where  $L$  is the channel width. Therefore, coupling Eqs. (2) and (3) allows to compute (numerically)  
143 the parameter  $W$ .

144 Since the satellites provide the water surface elevation,  $h$ , from altimeter and mean flow velocity,  $v$ ,  
145 from MODIS, the entropic method needs further assumptions.

146 The flow depth,  $D$ , is computed as  $h-z_0$ , where  $z_0$  is the elevation of the channel bottom level.  $v_{maxS}$  is  
147 inferred from the mean flow velocity as  $v_{maxS}=v/\Phi$  (Chiu, 1989).  $\Phi$  is a parameter found to be constant  
148 for a given river and ranging between 0.5-0.7 in different regions (Moramarco et al., 2004;  
149 Moramarco et al., 2011; Ammari and Remini, 2010). Nevertheless, in most cases presented in  
150 literature a value around 0.67 can be efficiently employed in ungauged river site.

151 The channel width,  $L$ , is assumed here as a constant and corresponds to the bankfull discharge. In this  
152 analysis the information coming from Google Earth  $\hat{I}$  is considered. The approach is found able to  
153 accurately model the surveyed flow area and assess the corresponding discharge by coupling the flow  
154 depth distribution and the surface flow velocity.

## 155 **2.5 Performance scores**

156 The accuracy of the water level and discharge estimates is determined by using different  
157 performance measures: coefficient of correlation,  $r$ , root mean square error,  $RMSE$  and Nash-Sutcliffe  
158 efficiency coefficient,  $NS$  (Nash and Sutcliffe, 1970), the mean absolute error,  $MAE$  and (for  
159 discharge) the relative root mean square error,  $RRMSE$ , defined as follows:

$$160 \quad RRMSE = \frac{RMSE}{\bar{Q}_{obs}} \cdot 100 \quad (2)$$

161 where  $\bar{Q}_{obs}$  is the mean value of the observed discharge.  $RRMSE$  ranges from 0 to  $\hat{O}$ , where 0 is the  
162 perfect match between the model and observations.

163

### 3. STUDY AREA AND *IN-SITU* DATASET

164 The study area is the Po River, in Northern Italy, located in the center of a large flat alluvial  
165 plain, the Pianura Padana (i.e. the Po river Valley). For this study, only the gauged station of  
166 Pontelagoscuro, subtending a drainage area equal to 70,091 km<sup>2</sup>, is used (see Figure 1). The geometric  
167 characteristics of the gauging station are derived through a ground survey carried out by the  
168 Interregional Agency of the River Po in 2005. In particular, the bankfull width and depth are equal to  
169 302 m and 18.73 m, respectively. The Pontelagoscuro station is used for the comparison of the  
170 simulated discharges. However, the analysis is carried out considering the VS where the altimetry  
171 satellite track overpasses the river and the characteristics of the section are 378 m and 13.20 m for  
172 the bankfull width and depth, respectively.

173 More than five years of daily data of water level,  $h$ , from February 2005 to August 2010, are  
174 selected for Pontelagoscuro station. The river discharge,  $Q$ , at the selected gauging station is derived  
175 through a rating curve obtained by the contemporary water level and velocity measurements,  
176 occasionally collected for different discharge conditions. The mean flow velocity is computed as the  
177 ratio between  $Q$  and the river section area  $A$ , where  $A$  is calculated as a function of the water level,  $A$   
178  $= f(h)$ .

179

### 4. REMOTE SENSING DATASET

180 As regards the altimetry data, we used River - Lake Hydrology (RLH) products provided by de  
181 Montfort University, UK, on behalf of ESA (<http://earth.esa.int/riverandlake>). We consider the track  
182 315, henceforth named as virtual station (VS), as the location where data derived from ENVISAT are  
183 available (Figure 1).

184 MODIS channel 1 (0.620-0.670  $\mu\text{m}$   $\delta$  Red) and channel 2 (0.841-0.876  $\mu\text{m}$   $\delta$  Near Infrared) at  
185 250 m of spatial resolution were extracted from MODIS Level 1B (MYD02QKM) datasets, acquired



186 by the sensor aboard Aqua satellite in the same period (February 2005 - August 2010). The images  
187 from MODIS are available every day, whereas the altimetry data are provided every 35 days.

## 188 5. RESULTS AND DISCUSSION

### 189 5.1 Comparison of *in-situ* and altimetry water level

190 The altimetry data from VS are compared with the *in-situ* water level, removing the average  
191 values of both the time series (Figure 2). As the section of Pontelagoscuro is located about 30 km  
192 downstream the VS and the time delay between the virtual and the *in-situ* station is less than one day,  
193 the observed and altimetry water levels can be considered simultaneous. The altimetry data are in  
194 good agreement with the observed data with a coefficient of correlation of 0.88 and the *NS* equal to  
195 0.78. The estimated *RMSE* is equal to 0.70 m, consistently with previous studies. For example,  
196 Birkinshaw et al. (2010) found *RMSE* values in the range 0.44-0.65 m along the Mekong river  
197 (Malaysia), whereas Bercher and Kosuth (2012) found an average *RMSE* value of about 0.73 m on  
198 27 VSs considering ENVISAT satellite data in Amazon basin.

### 199 5.2 Evaluation of mean flow velocity for the VS

200 All the images of MODIS onboard Aqua acquired in the period 2005-2010 over Northern Italy  
201 are firstly processed obtaining surface reflectance values ( $R_1$  and  $R_2$ ). Successively, for each image,  
202 a box with dimensions of 29x33 pixels centred at the VS is extracted (the dashed box in Figure 1)  
203 obtaining globally 4764 sub-scenes (2382 for  $R_1$  and 2382 for  $R_2$ ), almost one per day. After the cloud  
204 detection, the number of  $R_2$  images selected is 1121, equal to 47% of the total (2382), representing a  
205 huge and robust sample of data.

206 To identify the best locations for the pixels  $C$  and  $M$ , we follow the approach described in  
207 Tarpanelli et al. (2013b) for which the urban areas (or areas with temporal coefficients of variation,  
208  $CV$ , less than 0.4) and the meanders are considered as the best locations for the position of the pixels  
209  $C$  and  $M$ , respectively. Following the above guidelines, the pixel  $C$  is taken in the upper part of the

210 box, where the  $CV$  is low ( $CV = 0.37$ ) and an urban area is present, and  $M$  is located very near the  
211 river as shown in Figure 3a. Successively, the ratio  $C/M$  is calculated considering the temporal series  
212 of the selected pixels. In order to reduce the effects of the short term and observation noises, the  
213 exponential smoothing filter is applied choosing  $T$ -value equal to 20 days (comparable to the revisit  
214 time of the Aqua satellite equal to 16 days). As a result, once  $C/M^*$  time series is identified, the mean  
215 flow velocity can be estimated, by applying the regional relationship (Eq. (1)). Figure 3b shows the  
216 comparison between the  $C/M^*$  and the  $v$  time series, normalized to identify approximately the same  
217 range of variability. The  $C/M^*$  index closely follows the seasonal pattern of  $v$  with higher values in  
218 the winter season and lower in summer. Interestingly, MODIS-derived data are also able to identify  
219 the difference in the  $v$  values among the different years. In fact, in the period 2005-2007 the  $C/M^*$   
220 values were considerably lower than in 2009 and 2010, in good accordance with the *in-situ*  
221 observations. Nonetheless, the discrepancies, as for instance, in the second half of 2007, between the  
222 two time series highlight the residual noise not accounted for in the developed procedure.

### 223 **5.3 Evaluation of mean flow area by using entropic approach**

224 The mean flow velocity derived by MODIS is here used for estimating the maximum surface  
225 velocity. Generally, the ratio between the mean and the maximum velocity for different flow regimes  
226 is found constant and for the Po River is equal to 0.668 (Moramarco et al., 2011). As above specified,  
227 a value of 0.67 might be assumed if no measurements are available in the study area. Assuming the  
228 surface velocity distribution as an elliptical profile, the maximum surface flow velocity for each  
229 vertical is calculated and used in the entropy flow depth distribution. As regards the entropy  
230 parameter,  $W$ , which is an indicator of ratio between the mean and maximum flow depth, it is  
231 calculated coupling equations 2 and 3. For the Po River the value of  $W$  is found more than twice the  
232 ones obtained by Moramarco et al. (2013) for narrower rivers (e.g. Tiber River, from 30 to 70 m)  
233 compared to the Po River (~300 m). Specifically, the width of the Po River at the VS has been  
234 extracted by Google Earth  $\hat{I}$  and is equal to 352 m.

235 For the estimation of maximum flow depth, we assumed the bottom level at the centre of the  
236 cross section to be known. From the water level derived by satellite altimetry, Eq.(1) is used for  
237 estimating the flow depth distribution. Concerning the calculation of the cross section flow area  $A$ ,  
238 this is addressed by integrating Eq.(1) along the river cross section. Therefore, for each measurement  
239 of velocity and water level, an estimation of flow area is provided.

240 The flow area calculated following the entropy approach is very well predicted (the  $RMSE$  value  
241 is  $43 \text{ m}^2$ , whereas the  $RRMSE$  is about 3%). This result confirms the reliability of the assumption for  
242 considering the central point as the point where the maximum depth occurs.

#### 243 **5.4 River discharge estimation by coupling altimetry and MODIS data**

244 In Tarpanelli et al. (2013b) the discharge is inferred as the product of the velocity derived by  
245  $C/M^*$  according to the regional relationship and the flow area estimated considering the water levels  
246 measured *in-situ*. In this analysis, for the estimation of the river discharge two cases are analyzed: 1)  
247 the cross section geometry is available from *in-situ* survey, 2) the cross section geometry is  
248 reconstructed through the entropy approach. In both cases, the flow area is estimated considering the  
249 water level derived from satellite altimetry. Similarly to the water levels, the simulated discharges are  
250 also compared to the ones observed in the nearest *in-situ* gauged station of Pontelagoscuro, in the  
251 same day of observation.

252 In the case of known bathymetry, the comparison between the observed and simulated  
253 discharges reported in Figure 4 shows a slight overestimate for low flows and an underestimate for  
254 high flows. The latter result is expected as MODIS is unable to detect the reflectance value during  
255 high flows or flood event because of the high probability of cloud cover (Khan et al., 2012). However,  
256 the performance of the proposed approach is quite good with coefficient of correlation equal to 0.91  
257 and  $RMSE$  and  $RRMSE$  equal to  $423 \text{ m}^3\text{s}^{-1}$  and 36%, respectively (see Table 1). The analysis is carried  
258 out also choosing other locations for  $M$  and  $C$  (not shown for brevity) and very similar results are  
259 obtained.

260 In the second case, in which the cross section geometry is reconstructed through the entropy  
261 approach, the results in terms of discharge worsened remaining very close to those obtained by  
262 considering the geometry of the actual cross-section (see Table 1). The coefficient of correlation  
263 remains high and equal to 0.91, whereas the *RMSE* increases and the Nash Sutcliffe decreases. The  
264 error on the discharge of about 38% is a good result considering that only a ground point (the middle  
265 point elevation of the cross-section) was used in the analysis.

266 In order to evaluate the different error sources for assessing the discharge, a further analysis,  
267 exploiting satellite data in a separate way, is carried out. In particular, the discharge is evaluated with  
268 two different approaches: 1) by the product of the MODIS-derived velocity and the "observed" flow  
269 area, namely  $Q_{MODIS}$  and 2) by the product of the "observed" mean flow velocity and the flow area  
270 determined considering the satellite altimetry-derived water level, namely  $Q_{ALT}$ . The discharge  
271 observed at Pontelagoscuro gauged station is assumed as a benchmark. The "observed" flow area and  
272 "observed" mean flow velocity are computed at the gauged station, whereas the satellite data (velocity  
273 and water level) refer to the VS. In both cases, the actual cross sections are considered in the analysis.  
274 As shown in Table 1, the maximum source of error is due to the velocity derived by MODIS with the  
275 *RRMSE* equal to 43%. Although the error on the velocity is quite high, in the final evaluation of the  
276 discharge this aspect is compensated by the good performance of the altimetry that provides lower  
277 error (*RRMSE* = 22%). Indeed, the river discharge obtained through MODIS and altimetry data,  
278  $Q_{MODIS}$  (blue line in Figure 5a), is strongly affected by the error on the velocity derived by MODIS,  
279 leading an overestimation for low flow, as for example in the 2006 and 2007, and an underestimation  
280 for high flow, as shown for the peak discharge in 2008 and 2010 (see also Figure 5b). On the contrary  
281 the use of altimetry with the "observed" cross section and the "observed" mean flow velocity gives  
282 very good results as shown by the red circle lying above the bisector in Figure 5b. As an explanation,  
283 it should be stressed that one possible residual source of error could be related to the MODIS data  
284 reprojection operation. This procedure needs when spatially co-located series of data have to be  
285 analyzed. When data are acquired at very high zenithal angle, the actual spatial resolution is higher

286 than the nominal one (i.e. 1km at Nadir for MODIS), so that during the reprojection of these data a  
287 smoothing of the detected reflectance value may be possible. It is expected that further studies on the  
288 topic for deriving mean flow velocity from MODIS and the future Sentinel-3 mission, in which a  
289 visible-near infrared multispectral sensor (i.e. the Ocean and Land Colour Instrument, OLCI) and an  
290 altimeter (i.e. the Sentinel-3 Ku/C Radar Altimeter, SRAL) may contribute to the improvement of the  
291 proposed procedure. Indeed, the two sensors will provide data with both better vertical accuracy (total  
292 range error up to 3 cm) and higher spatial (inter-track separation at the equator of 52 km) and temporal  
293 resolution (27 days for SRAL with 2 satellites); besides, being onboard the same satellite platform,  
294 the issue of having simultaneous measurements will be solved.

## 295 6. CONCLUSIONS

296 A study addressed to evaluate the potential of satellite data for estimation of the discharge in  
297 poorly gauged river sites is presented in this paper. Specifically, the discharge is assessed as the  
298 product of the flow velocity derived from MODIS and the flow area, calculated as a function of the  
299 water levels derived from the radar altimeter onboard ENVISAT satellite.

300 The obtained good results (relative root mean square error of about 37% and a correlation of  
301 0.91 with in-situ measurements) demonstrate the potential of coupling the two satellite sensors to  
302 calculate the discharge. The procedure can be applied also when the river section geometry is  
303 unknown by using the entropy approach proposed by Moramarco et al. (2013) for estimating the river  
304 bathymetry from the flow velocity estimated by MODIS. However, the latter method needs the  
305 knowledge of at least one point of the bed level.

306 These aspects may be of particular interest in view of the next satellite mission Sentinel-3 for  
307 which the Ocean and Land Colour Instrument (OLCI) and the Sentinel-3 Ku/C Radar Altimeter  
308 (SRAL) will be onboard the same satellite thus solving the issue of having simultaneous  
309 measurements, with improvements in terms of both vertical accuracy and spatial and temporal  
310 resolution.

311

312 **Acknowledgments:** The authors wish to thank the European Space Agency for furnishing the  
313 altimetry data; Interregional Agency of the River Po (AIPO) and in particular, Eng. Federica  
314 Pellegrini, for providing the analyzed data for Po River basin.

## 315 REFERENCES

- 316 Albergel, C., Rüdiger, C., Pellarin, T., Calvet, J. C., Fritz, N., Froissard, F., Suquia, D., Petitpa, A.,  
317 Piguët, B., Martin, E., 2008. From near-surface to root-zone soil moisture using an exponential  
318 filter: An assessment of the method based on in-situ observations and model simulations.  
319 *Hydrology and Earth System Sciences*, 12, 1323-1337.
- 320 Alsdorf, D. E., Rodriguez, E., Lettenmaier, D. P., 2007. Measuring surface water from space. *Review*  
321 *of Geophysics*, 45, RG2002.
- 322 Ammari A., Remini B., 2010. Estimation of Algerian rivers discharges based one Chiuø equation.  
323 *Arabian Journal of Geosciences*, 3(1), 59-65.
- 324 Bercher, N., Kosuth, P., 2013. Monitoring river water levels from space: quality assessment of 20  
325 years of satellite altimetry data. *Proceeding -20 Years of Progress in Radar Altimetryø*, 24-29  
326 September 2012, Venice, Italy.
- 327 Biancamaria, S., Andreadis, K.M., Durand, M., Clark, E.A., Rodriguez, E., Mognard, N.M., Alsdorf,  
328 D.E., Lettenmaier, D.P., Oudin, Y., 2010. Preliminary Characterization of SWOT Hydrology Error  
329 Budget and Global Capabilities. *IEEE Journal of Selected Topics in Applied Earth Observations*  
330 *and Remote Sensing*, 3(1), 6 ó 19.
- 331 Birkett, C.M., 1998. Contribution of the TOPEX NASA radar altimeter to the global monitoring of  
332 large rivers and wetlands. *Water Resources Research*, 34(5), 1223-1239.
- 333 Birkinshaw, S.J., O'Donnell, G.M., Moore, P., Kilsby, C.G., Fowler, H.J., Berry, P.A.M., 2010. Using  
334 satellite altimetry data to augment flow estimation techniques on the Mekong River. *Hydrological*  
335 *Processes*, 24, 3811-3825.
- 336 Bjerklie, D. M., Dingman, S. L., Vorosmarty, C. J., Bolster, C. H., Congalton, R. G., 2003. Evaluating  
337 the potential for measuring river discharge from space. *Journal of Hydrology*, 278, 17638.
- 338 Brakenridge, G. R., Anderson, E., 2006. MODIS-based flood detection, mapping and measurement:  
339 the potential for operational hydrological applications. *Proceedings of the NATO on*  
340 *Transboundary floods: reducing risk through flood management*, Eds. Marsalek J., Stancalie G.,  
341 Balint G., 72, 1-12.
- 342 Brakenridge, G. R., Nghiem, S. V., Anderson, E., Mic, R., 2007. Orbital microwave measurement of  
343 river discharge and ice status. *Water Resources Research*, 43, W04405.
- 344 De Oliveira Campos, I, Mercier, F., Maheu, C., Cochonneau, G., Kosuth, P., Blitzkow, D.,  
345 Cazenave, A., 2001. Temporal variations of river basin waters from Topex/ Poseidon satellite  
346 altimetry. Application to the Amazon basin. *Comptes Rendus de l'Académie des Sciences ó*  
347 *Serie IIA ó Earth and Planetary Science*, 333 (10), 633-643.
- 348 Durand, M., Rodriguez, E, Alsdorf, D.E., Trigg, M., 2010. Estimating river depth from remote  
349 sensing swath interferometry measurements of river height, slope, and width. *IEEE Journal*  
350 *of selected topics in applied earth observations and remote sensing*, 3(1), 20-31.
- 351 Frappart, F., Calmant, S., Cauhope, M., Seyler, F., Cazenave, A., 2006. Preliminary results of

- 352 ENVISAT RA-2-derived water levels validation over the Amazon basin. *Remote Sensing of*  
353 *Environment*, 100, 252-264.
- 354 Fu, L. Alsdorf, D. Morrow, R. Rodriguez, E. Mognard, N., 2012. SWOT: The Surface Water  
355 and Ocean Topography Mission: Wide-Swath Altimetric Measurement of Water Elevation on  
356 Earth, Pasadena, CA, USA: Jet Propulsion Laboratory.
- 357 Getirana, A.C.V., Bonnet, M. P., Calmant, S., Roux, E., Rotunno, O. C., Mansur, W. J., 2009.  
358 Hydrological monitoring of poorly gauged basins based on rainfall-runoff modeling and  
359 spatial altimetry. *Journal of Hydrology*, 379, 205-219.
- 360 Getirana, A.C.V., Boone, A., Yamazaki, D., Mognard, N., 2013. Automatic parameterization of  
361 a flow routing scheme driven by radar altimetry data: Evaluation in the Amazon basin. *Water*  
362 *Resources Research*, 49(1), 614-629.
- 363 Khan, S.I., Hong, Y., Vergara, H.J., Gourley, J.J., Brakenridge, G.R., De Groeve, T., Flamig,  
364 Z.L., Policelli, F., Yong, B., 2012. Microwave Satellite Data For Hydrologic Modeling In  
365 Ungauged Basins. *IEEE Geoscience and Remote Sensing Letters*, 9(4), 663-667.
- 366 Koblinsky, C. J., Clarke, R. T., Brenner, A. C., Frey, H., 1993. Measurement of River Level  
367 variations with Satellite Altimetry. *Water Resources Research*, 29, 1839-1848.
- 368 Leon, J. G., Calmant, S., Seyler, F., Bonnet, M. P., Cauhope, M., Frappart, F., Filizola, N.,  
369 Fraizy, P., 2006. Rating curves and estimation of average water depth at the upper Negro  
370 River based on satellite altimeter data and modeled discharges. *Journal of Hydrology*, 328,  
371 481-496.
- 372 Michailovsky, C. I., Milzow, C., Bauer-Gottwein, P., 2013. Assimilation of radar altimetry to a  
373 routing model of the Brahmaputra River. *Water Resources Research*, 49(8), 480764816.
- 374 Moramarco T., Saltalippi C., Singh V.J., 2004. Estimating the cross-sectional mean velocity in  
375 natural channels using Chiou's velocity distribution. *Journal of Hydrologic Engineering*, 9,  
376 42650.
- 377 Moramarco, T., Saltalippi, C., Singh, V.J., 2011. Velocity profiles assessment in natural  
378 channels during high floods. *Hydrology Research*, 42 (2-3), 1626170.
- 379 Moramarco, T., Corato, G., Melone, F., Singh, V.P., 2013. An entropy-based method for  
380 determining the flow depth distribution in natural channels. *Journal of Hydrology*, 497,176-  
381 188.
- 382 Nash, J.E., Sutcliffe, J.V., 1970. River flow forecasting through conceptual models, Part I: A  
383 discussion of principles. *Journal of Hydrology*, 10(3), 282-290.
- 384 Santos da Silva, J., Calmant, S., Seyler, F., Rotunno Filho, O.C., Cochonneau, G., Mansur, W.J.,  
385 2010. Water levels in the Amazon basin derived from the ERS 2 and ENVISAT radar  
386 altimetry missions. *Remote Sensing of Environment*, 114, 2160-2181.
- 387 Smith, L. C., Pavelsky, T. M., 2008. Estimation of river discharge, propagation speed, and  
388 hydraulic geometry from space: Lena River, Siberia. *Water Resources Research*, 44, W03427.
- 389 Tarpanelli, A., Barbetta, S., Brocca, L., Moramarco, T., 2013a. River discharge estimation by  
390 using altimetry data and simplified flood routing modeling. *Remote Sensing*, 5(9), 414564162.
- 391 Tarpanelli, A., Brocca, L., Melone, F., Moramarco, T., Lacava, T., Faruolo, M., Pergola, N.,  
392 Tramutoli, V., 2013b. Toward the estimation of river discharge variations using MODIS data  
393 in ungauged basins. *Remote Sensing of Environment*, 136, 47-55.
- 394 Temimi, M., Leconte, R., Brissette, F., Chaouch, N., 2007. Flood and soil wetness monitoring over  
395 the Mackenzie River Basin using AMSR-E 37 GHz brightness temperature. *Journal of Hydrology*,  
396 333, 3176328.
- 397 Temimi, M., Romanov, P., Ghedira, H., Khanbilvardi, R., Smith, K., 2011. Sea ice monitoring over

- 398 the Caspian Sea using geostationary satellite data. *International Journal of Remote Sensing*, 32(6).
- 399 Tourian M.J., Sneeuw, N., Bardossy A., 2013. A quantile function approach to discharge estimation  
400 from satellite altimetry (ENVISAT). *Water Resources Research*, 49(7), 4174 - 4186.
- 401 Yoon, Y., Durand, M., Merry, C.J., Rodriguez, E., 2013. Improving Temporal Coverage of the SWOT  
402 Mission Using Spatiotemporal Kriging. *IEEE Journal of Selected Topics in Applied Earth  
403 Observations and Remote Sensing*, 6(3), 1719 ó 1729.
- 404 Wagner, W., Lemoine, G., Rott, H., 1999. A method for estimating soil moisture from ERS  
405 scatterometer and soil data. *Remote Sensing of Environment*, 70, 191-207.
- 406 Zakharova, E.A., Kouraev, A.V., Cazenave, A., Seyler F., 2006. Amazon River discharge estimated  
407 from TOPEX/Poseidon altimetry. *Comptes Rendus Geoscience*, 338, 188-196.



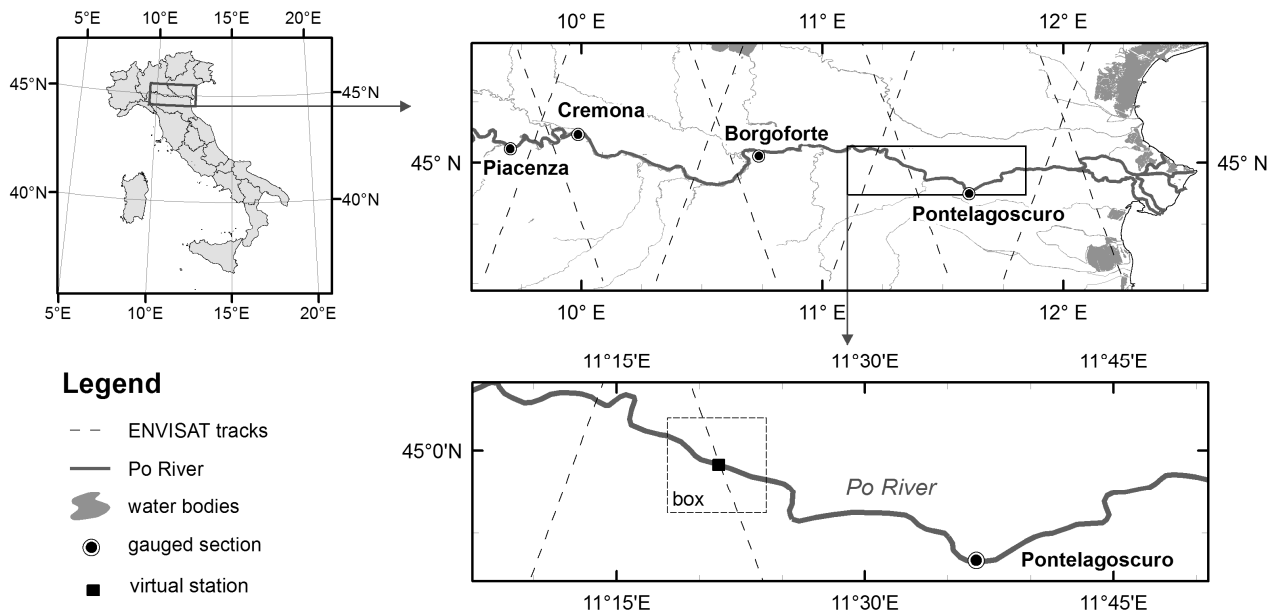
## 408 TABLES

409 **Table 1** Comparison between the discharges calculated by using the actual and reconstructed cross section  
 410 and the ones observed at Pontelagoscuro gauged section (*RMSE* = root mean square error; *NS* = Nash  
 411 Sutcliffe efficiency; *RRMSE* = relative root mean square error; *MAE* = mean absolute error). For symbol,  
 412 please see text.

<b>DISCHARGE</b>	<b>RMSE (<math>\text{m}^3\text{s}^{-1}</math>)</b>	<b>NS (-)</b>	<b>RRMSE (%)</b>	<b>MAE (<math>\text{m}^3\text{s}^{-1}</math>)</b>
<i>Q<sub>MODIS</sub></i> (Actual geometry)	506	0.65	43	447
<i>Q<sub>ALT</sub></i> (Actual geometry)	259	0.90	22	165
<i>Q<sub>MODIS+ALT</sub></i> (Actual geometry)	415	0.75	36	346
<i>Q<sub>MODIS+ALT+ENTR</sub></i> (Reconstructed geometry)	448	0.72	38	363

413

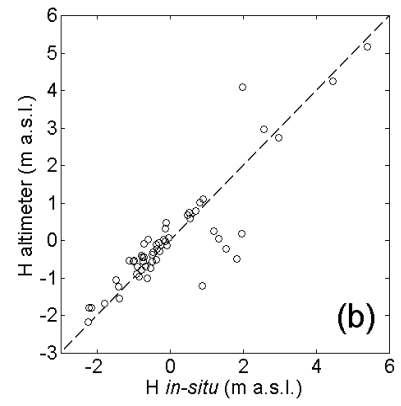
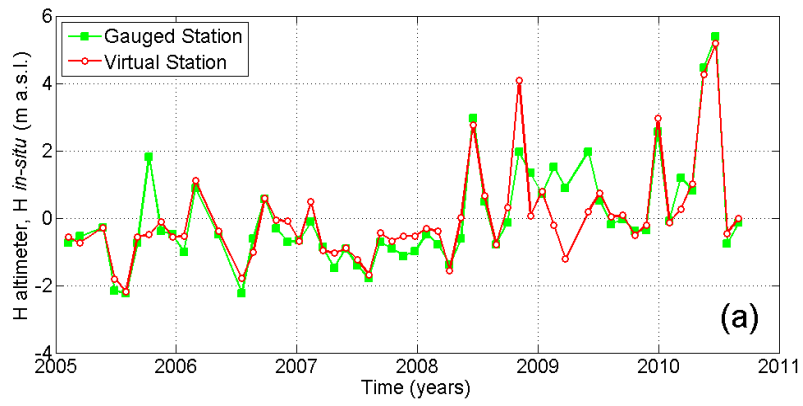
414 FIGURES



415

416 **Figure 1.** Location of the Po River study area. The ENVISAT satellite tracks, the Pontelagoscuro gauged  
417 section and the box used for the MODIS data analysis are also shown.

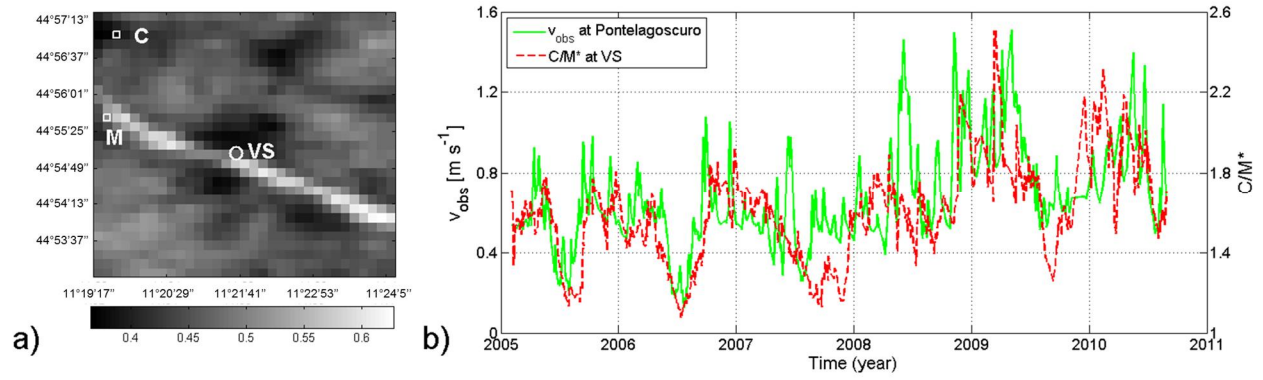
418



419

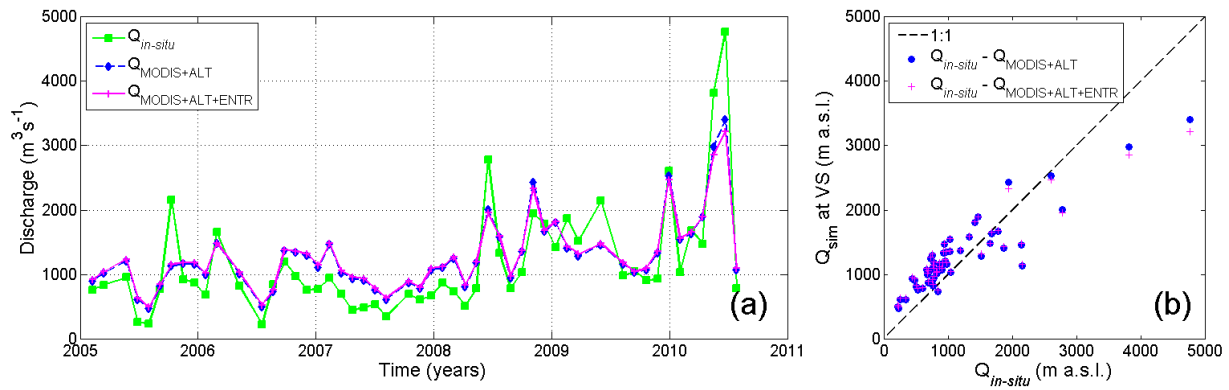
420 **Figure 2.** Comparison between the water levels recorded at the *in-situ* gauged station of Pontelagoscuro and  
 421 the ones provided at the virtual station (VS) by ENVISAT RA-2.

422



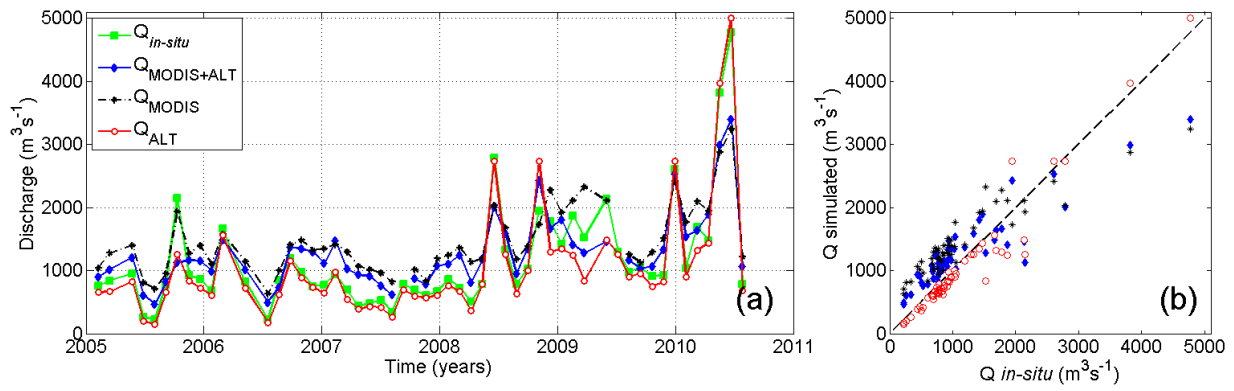
423

424 **Figure 3.** a) Map of temporal coefficients of variation of the reflectance values of the box VS shown in Figure  
 425 1; b) Comparison between the temporal series of mean flow velocity observed at Pontelagoscuro,  $v_{obs}$ , and of  
 426 the MODIS ratio  $C/M^*$ .



427

428 **Figure 4.** Comparison in terms of the temporal series a) and the scatter plot b) between the discharge observed  
 429 at Pontelagoscuro gauged station,  $Q_{in-situ}$ , and the one simulated at the virtual station VS,  $Q_{sim}$ , by considering  
 430 the actual section geometry,  $Q_{MODIS+ALT}$ , and the one derived by the entropy approach  $Q_{MODIS+ALT+ENTR}$ .



431

432 **Figure 5.** Comparison in terms of the temporal series a) and the scatter plot b) between the discharge observed  
 433 at Pontelagoscuro gauged station,  $Q_{in-situ}$ , and the ones simulated at the virtual station VS, by considering the  
 434 actual section geometry,  $Q_{MODIS+ALT}$ ,  $Q_{MODIS}$  and  $Q_{ALT}$ . For symbol see text.

435